General considerations for the miniaturization of radiating antennae

Yan Francescato,[1,2] Jingjing Yang,[1] Ming Huang,[1]* and Stefan A. Maier[2]

[1] *Wireless Innovation Lab of Yunnan University, Kunming 650091, People's Republic of China*
[2] *The Blackett Laboratory, Imperial College London, London SW7 2AZ, United Kingdom*

*huangming@ynu.edu.cn

Abstract: The small size of plasmonic nanostructures compared to the wavelength of light is one of their most distinct and defining characteristics. It results in the strong compression of an incident wave to intense hot spots which have been used most remarkably for molecular sensing and nanoscale lasers. But another important direction for research is to use this ability to design miniaturized interconnects and modulators between fast, loss-less photonic components. In this situation one is looking for the smallest optical nanostructure possible while trying to mitigate losses. Here we show that despite their high absorption, conductors are still the best materials to reach the sub-wavelength regime for optical antennae when compared to polar crystals and high-index dielectrics, two classes of material which have shown a lot of potential recently for nanophotonic applications. It is demonstrated through both Mie theory and numerical calculations that the smallest possible, efficient, radiating antenna has a length $L > \lambda_{res}/20$ in all cases (this length is typically $L = \lambda_{res}/2$ in microwave engineering), including the redshifting mechanism induced by a background or substrate refractive index, the effect of material loss and that of shape. In addition, we show that although the assembly of individual particles can further increase the miniaturization factor, it strongly increases the size-mismatch in detriment of the overall efficiency, thus making this method unfit for radiating antennae. By identifying the relevant dimensionless properties for conductors, polar materials and high index dielectrics, we present an unified understanding of the behaviour of sub-wavelength nanostructures which are at the heart of current nanophotonic research and cast the upper achievable limits for optical antennae crucial to the development of real-life implementation.

OCIS codes: (350.4238) Nanophotonics and photonic crystals, (160.4670) Optical materials, (290.4020) Mie theory.

References and links

1. E. Ozbay, "Plasmonics: Merging photonics and electronics at nanoscale dimensions," Science **311**, 189–193 (2006).
2. W. L. Barnes, A. Dereux, and T. W. Ebbesen, "Surface plasmon subwavelength optics," Nature **424**, 824–830 (2003).
3. A. Alù and N. Engheta, "Wireless at the nanoscale: Optical interconnects using matched nanoantennas," Phys. Rev. Lett. **104**, 213902 (2010).

4. P. Biagioni, J.-S. Huang, and B. Hecht, "Nanoantennas for visible and infrared radiation," Reports on Progress in Physics **75**, 024402 (2012).
5. M. Agio, "Optical antennas as nanoscale resonators," Nanoscale **4**, 692–706 (2012).
6. L. Novotny and N. van Hulst, "Antennas for light," Nature Photonics **5**, 83–90 (2011).
7. V. Giannini, A. I. Fernández-Domínguez, S. C. Heck, and S. A. Maier, "Plasmonic nanoantennas: Fundamentals and their use in controlling the radiative properties of nanoemitters," Chemical Reviews **111**, 3888–3912 (2011).
8. F. Neubrech, A. Pucci, T. W. Cornelius, S. Karim, A. Garcia-Etxarri, and J. Aizpurua, "Resonant plasmonic and vibrational coupling in a tailored nanoantenna for infrared detection," Physical Review Letters **101** (2008).
9. M. D. Sonntag, J. M. Klingsporn, A. B. Zrimsek, B. Sharma, L. K. Ruvuna, and R. P. Van Duyne, "Molecular plasmonics for nanoscale spectroscopy," Chem. Soc. Rev. **43**, 1230–1247 (2014).
10. R. Bardhan, S. Lal, A. Joshi, and N. J. Halas, "Theranostic Nanoshells: From Probe Design to Imaging and Treatment of Cancer," Accounts of Chemical Research **44**, 936–946 (2011).
11. J. M. Luther, P. K. Jain, T. Ewers, and A. P. Alivisatos, "Localized surface plasmon resonances arising from free carriers in doped quantum dots," Nature Materials **10**, 361–366 (2011).
12. G. Georgiou, H. K. Tyagi, P. Mulder, G. J. Bauhuis, J. J. Schermer, and J. G. Rivas, "Photo-generated THz antennas," Scientific Reports **4** (2014).
13. F. H. L. Koppens, D. E. Chang, and F. J. García de Abajo, "Graphene plasmonics: A platform for strong light-matter interactions," Nano Letters **11**, 3370–3377 (2011).
14. J. Chen, M. Badioli, P. Alonso-Gonzalez, S. Thongrattanasiri, F. Huth, J. Osmond, M. Spasenovic, A. Centeno, A. Pesquera, P. Godignon, A. Zurutuza Elorza, N. Camara, F. Javier García de Abajo, R. Hillenbrand, and F. H. L. Koppens, "Optical nano-imaging of gate-tunable graphene plasmons," Nature **487**, 77–81 (2012).
15. Z. Fei, A. S. Rodin, G. O. Andreev, W. Bao, A. S. McLeod, M. Wagner, L. M. Zhang, Z. Zhao, M. Thiemens, G. Dominguez, M. M. Fogler, A. H. C. Neto, C. N. Lau, F. Keilmann, and D. N. Basov, "Gate-tuning of graphene plasmons revealed by infrared nano-imaging," Nature **487**, 82–85 (2012).
16. J. A. Schuller, T. Taubner, and M. L. Brongersma, "Optical antenna thermal emitters," Nature Photonics **3**, 658–661 (2009).
17. Y. Chen, Y. Francescato, J. D. Caldwell, V. Giannini, T. W. W. Ma, O. J. Glembocki, F. J. Bezares, T. Taubner, R. Kasica, M. Hong, and S. A. Maier, "Spectral tuning of localized surface phonon polariton resonators for low-loss mid-ir applications," ACS Photonics **1**, 718–724 (2014).
18. J. A. Schuller and M. L. Brongersma, "General properties of dielectric optical antennas," Opt. Express **17**, 24084–24095 (2009).
19. A. García-Etxarri, R. Gómez-Medina, L. S. Froufe-Pérez, C. López, L. Chantada, F. Scheffold, J. Aizpurua, M. Nieto-Vesperinas, and J. J. Sáenz, "Strong magnetic response of submicron silicon particles in the infrared," Opt. Express **19**, 4815–4826 (2011).
20. A. E. Krasnok, A. E. Miroshnichenko, P. A. Belov, and Y. S. Kivshar, "All-dielectric optical nanoantennas," Optics Express **20**, 20599–20604 (2012).
21. Y. H. Fu, A. I. Kuznetsov, A. E. Miroshnichenko, Y. F. Yu, and B. Luk'yanchuk, "Directional visible light scattering by silicon nanoparticles," Nature Communications **4** (2013).
22. L. Novotny, "Effective wavelength scaling for optical antennas," Phys. Rev. Lett. **98**, 266802 (2007).
23. L. Cao, P. Fan, E. S. Barnard, A. M. Brown, and M. L. Brongersma, "Tuning the color of silicon nanostructures," Nano Letters **10**, 2649–2654 (2010). PMID: 20507083.
24. J. M. Geffrin, B. Garcia-Camara, R. Gomez-Medina, P. Albella, L. S. Froufe-Perez, C. Eyraud, A. Litman, R. Vaillon, F. Gonzalez, M. Nieto-Vesperinas, J. J. Saenz, and F. Moreno, "Magnetic and electric coherence in forward- and back-scattered electromagnetic waves by a single dielectric subwavelength sphere," Nature Communications **3** (2012).
25. P. Albella, M. A. Poyli, M. K. Schmidt, S. A. Maier, F. Moreno, J. J. Senz, and J. Aizpurua, "Low-loss electric and magnetic field-enhanced spectroscopy with subwavelength silicon dimers," The Journal of Physical Chemistry C **117**, 13573–13584 (2013).
26. T. G. Habteyes, I. Staude, K. E. Chong, J. Dominguez, M. Decker, A. Miroshnichenko, Y. Kivshar, and I. Brener, "Near-field mapping of optical modes on all-dielectric silicon nanodisks," ACS Photonics **1**, 794–798 (2014).
27. A. E. Krasnok, C. R. Simovski, P. A. Belov, and Y. S. Kivshar, "Superdirective dielectric nanoantennas," Nanoscale **6**, 7354–7361 (2014).
28. Y. Yang, W. Wang, P. Moitra, I. I. Kravchenko, D. P. Briggs, and J. Valentine, "Dielectric meta-reflectarray for broadband linear polarization conversion and optical vortex generation," Nano Letters **14**, 1394–1399 (2014). PMID: 24547692.
29. U. Zywietz, A. B. Evlyukhin, C. Reinhardt, and B. N. Chichkov, "Laser printing of silicon nanoparticles with resonant optical electric and magnetic responses," Nature Communications **5** (2014).
30. P. Albella, R. Alcaraz de la Osa, F. Moreno, and S. A. Maier, "Electric and magnetic field enhancement with ultralow heat radiation dielectric nanoantennas: Considerations for surface-enhanced spectroscopies," ACS Photonics **1**, 524–529 (2014).
31. I. Staude, A. E. Miroshnichenko, M. Decker, N. T. Fofang, S. Liu, E. Gonzales, J. Dominguez, T. S. Luk, D. N. Neshev, I. Brener, and Y. Kivshar, "Tailoring directional scattering through magnetic and electric resonances in

subwavelength silicon nanodisks," ACS Nano **7**, 7824–7832 (2013).
32. R. Hillenbrand, T. Taubner, and F. Keilmann, "Phonon-enhanced light-matter interaction at the nanometre scale," Nature(London) **418**, 159–162 (2002).
33. C. Kittel, *Introduction to solid state physics* (John Wiley & Sons, Inc., New York, 1996).
34. C. F. Bohren and D. R. Huffman, *Absorption and Scattering of Light by Small Particles* (Wiley-VCH Verlag GmbH, 1998).
35. A. von Hippel, R. G. Breckenridge, F. G. Chesley, and L. Tisza, "High dielectric constant ceramics," Industrial and Engineering Chemistry **38**, 1097–1109 (1946).
36. T. Hamano, D. J. Towner, and B. W. Wessels, "Relative dielectric constant of epitaxial batio3 thin films in the ghz frequency range," Applied Physics Letters **83** (2003).
37. A. Demetriadou and O. Hess, "Analytic theory of optical nanoplasmonic metamaterials," Phys. Rev. B **87**, 161101 (2013).
38. J. van de Groep and A. Polman, "Designing dielectric resonators on substrates: Combining magnetic and electric resonances," Opt. Express **21**, 26285–26302 (2013).
39. J. Dorfmuller, R. Vogelgesang, W. Khunsin, C. Rockstuhl, C. Etrich, and K. Kern, "Plasmonic nanowire antennas: Experiment, simulation, and theory," Nano Letters **10**, 3596–3603 (2010).
40. N. Verellen, F. Lpez-Tejeira, R. Paniagua-Domnguez, D. Vercruysse, D. Denkova, L. Lagae, P. Van Dorpe, V. V. Moshchalkov, and J. A. Snchez-Gil, "Mode parity-controlled fano- and lorentz-like line shapes arising in plasmonic nanorods," Nano Letters **14**, 2322–2329 (2014).
41. Z. Li, S. Butun, and K. Aydin, "Touching gold nanoparticle chain based plasmonic antenna arrays and optical metamaterials," ACS Photonics **1**, 228–234 (2014).
42. V. Giannini, A. Berrier, S. M. Maier, J. Antonio Sanchez-Gil, and J. G. Rivas, "Scattering efficiency and near field enhancement of active semiconductor plasmonic antennas at terahertz frequencies," Optics Express **18**, 2797–2807 (2010).

1. Introduction

Plasmonics is a relatively new and striving field of research of which one important goal is that of merging photonic technology to electronic components [1]. This is traditionally achieved by using the field confinement capability of nanostructured metal where the coupling between the charge density fluctuations of the conduction electrons and electromagnetic waves results in bound modes called surface plasmon polaritons [2]. These extremely appealing excitations combine the properties of both photons and electric currents and are therefore foreseen as the most promising entities to achieve the aforementioned merging [3]. This has led to the concept of "optical" antennae which represents a scaling of the radio-frequency antennae down to submicrometer sizes in order to react to the wavelength of visible light [4, 5].

There is a strong deviation from microwave antenna theory as the driving frequency is increased caused by the so-called skin effect, which is an increased complex character of the conductivity of a metal [6]. This allows for an additional miniaturization which cannot take place in a near-perfect conductor and is the source of some of the most striking plasmonic applications, such as emitters engineering [7], surface-enhanced spectroscopy and molecular sensing [8, 9] or photothermal therapy [10], where optical antennae serve as an interface between the wavelength of light and the size of molecules. However, as the size-mismatch increases between the wavelength and the antenna size, the efficiency of the latter decreases in proportion; it results in smaller components but at the cost of additional dissipation. In the present article, we will explore the trade-off regime across a wide range of frequencies, looking for the smallest possible antenna with a workable efficiency which we define by dominating radiating properties compared to the absorption.

In recent years, researchers have identified alternative avenues to metals as a way to achieve light confinement. For instance, similarly to noble metals, semiconductors exhibit plasmonic properties which can be tuned across a wide spectral range, from the near-infrared down to the terahertz regime, simply by varying their carrier concentration [11, 12]. This is also the case for the promising 2D material graphene, where the atomic thickness can produce an unprecedented compression of the field [13–15]. But polaritons, these surface modes binding light

to interfaces, can arise in polar crystals alike thanks to the stimulation of charged transverse optical phonons [16, 17]. Finally, the use of high refractive index dielectrics can give rise to gigantic sub-wavelength hot spots [18–21]. Because the compression of light in these systems originates from different physical mechanisms, we can expect different figures of merit for the miniaturization of antennae and therefore we will explore those in detail in the following.

We will start by using Mie theory, investigating the first order resonance supported by small spheres made out of these materials. This will allow to analyze in detail the effect of the material properties as well as the achievable radiation efficiency and miniaturization of these systems. Next, we will consider the case of elongated particle through finite-difference time domain (FDTD) calculations and making use of the effective wavelength theory developed by Novotny [22]. Last, we will study the influence of the background refractive index and the redshift caused by the assembling of particles.

2. Materials under investigation

We choose to investigate here the performance of three categories of materials in which the compression of free-space light is achieved through completely different physical effects in order to cover as vast a ground as possible. First of all, we consider the modes supported by high-index dielectrics (HID) which have experienced recently a surge in popularity within the nanophotonic community [23–29]. This stems in large part because of their extremely small losses in the visible range making them attractive alternative to the predominant noble metals [30]. However, as we will see, as the wavelength of radiation increases dissipation in dielectrics can become relatively high although it is typically accompanied by large rise in the dielectric constant as well. The lowest order mode of a spherical dielectric particle is named the magnetic dipole (MD) and can be found at the wavelength $\lambda_{res} = nD$, where n is the index of the dielectric and D its diameter. This means that HID resonators can never beat the diffraction limit, however extremely high index can allow deeply sub-wavelength elements. Note that for low aspect ratio particles the electric dipole can even be located at higher frequency than the corresponding magnetic dipole [31]. More generally, the following relation describes the complex index $\tilde{n}$ of HID

$$\tilde{n}^2 = \varepsilon = \varepsilon'(1 + i\tan\delta) \quad \text{with} \quad \tan\delta = \varepsilon''/\varepsilon' \tag{1}$$

where the dielectric constant ε' and the loss tangent $\tan\delta$ are used in a similar fashion for high-k ceramics in microelectronics.

By far the most widely used materials for nanophotonics, conductors have risen as a powerful ingredients for sub-diffraction applications [2]. This originates from the stimulation of surface plasmons below the plasma frequency $\omega_p^2 = Nq_e^2/\varepsilon_0 m^*$, with N the charge carrier concentration, q_e and m^* the charge of the electron and effective mass of the charge carrier, and ε_0 the permittivity of free-space, which cause a formidable confinement of the incident light. The behaviour of conductors is well reproduced by a Drude model in the absence of interband transitions

$$\tilde{n}^2 = \varepsilon = \varepsilon_\infty - \frac{\omega_p^2}{\omega^2 + i\Gamma\omega} \tag{2}$$

with ε_∞ the permittivity due to the ion background and $\Gamma = 2\pi/\tau$ the charge carrier scattering rate (τ being the scattering time). While the performance of conductors decrease fast away from $\Re\{\varepsilon\} = -2$, *i.e.* above 600 nm for noble metals, the possibility to tune the carrier concentration N in semiconductors allow to span a large range of frequency from the near-infrared down to the terahertz regime.

Last, another class of emerging materials is that of polar crystals in which photons can couple to surface phonons rather than surface plasmons thanks to the charge carried by their transverse

lattice oscillations [32]. These are foreseen as promising components for plasmonic-like capabilities within the terahertz to mid-infrared ranges in which the optical phonons can be stimulated. They suffer from reduced absorption compared to conductors because of the absence of Joule heating, leading to scattering time two orders of magnitude longer; it is therefore important to realize that those materials exceed the performance of noble metals only when their operating frequency is more than a hundredth that of the visible range. A Drude-Lorentz model is used to describe their dielectric function

$$\tilde{n}^2 = \varepsilon = \varepsilon_\infty + \frac{\varepsilon_\infty(\omega_{LO}^2 - \omega_{TO}^2)}{\omega_{TO}^2 - \omega^2 - i\Gamma\omega} \quad \text{with} \quad \frac{\omega_{LO}^2}{\omega_{TO}^2} = \frac{\varepsilon_{st}}{\varepsilon_\infty} \sim 1.44 \tag{3}$$

with ω_{LO} and ω_{TO} the longitudinal and transverse optical phonon frequencies. We see that the permittivity is only negative, *i.e.* with a plasmonic-like behaviour, in between these two phonon modes which consists in the most severe limitation of polar crystals. Indeed, that frequency range is fixed for each material and rather reduced, as attested by the Lyddane-Sachs-Teller (LST) relationship $\omega_{LO}^2/\omega_{TO}^2 = \varepsilon_{st}/\varepsilon_\infty$ [33]. Although it can be as high as 9 for very ionic materials such as fluorides, bromides or chlorides, it is way below 2 for most practical cases like silicon carbide or boron nitride. Given the strong absorption band at the TO frequency, we can already see that any redshifting mechanism will be detrimental to this category of material and it is therefore most useful for deeply sub-wavelength resonators.

3. Results and discussion

The total amount of light interacting with a particle is termed the extinction cross-section and is given by $C_{ext} = C_{abs} + C_{sca}$, with C_{abs} and C_{sca} the absorption and scattering contributions. One also refers to the optical efficiencies $Q_i = C_i/A$ which quantify the relative capture area of a particle relative to its physical cross-section A [7]. While it is well-known that in very small size "plasmonic" nanoparticles, most of the captured light is absorbed, we will focus here on antenna applications. This implies that the radiative contribution C_{sca} should dominate the optical process, *i.e.* that the radiative efficiency $\eta = C_{sca}/C_{ext} \geq 50\%$, which puts a limit on the miniaturization. We note however that small particles remain crucial for schemes such as molecular sensing or photothermal therapy.

3.1. Spherical particles

We consider first the case of spherical particles as it allows us to make use of Mie theory [34]. As we will see, this analytical framework provides us with a good general understanding of the effect of losses, size and the behaviour of the dielectric function. We will turn to the case of elongated particles, namely rods, in the subsequent subsection.

Fig. 1a reports the lowest energy resonance wavelength of dielectric spheres with radius $R = 10\,\mu$m and permittivity given by equation 1 with the real and imaginary part varying along the horizontal and vertical axis respectively. More precisely, the colormap represents the dimensionless quantity $\lambda_{res}/2R$ which defines the miniaturization factor. These results are therefore scalable across the whole electromagnetic spectrum as long as the value of the complex permittivity is similar. Furthermore, the benchmark value for this factor is $\lambda_{res}/L = 2$ corresponding to the resonance condition of the conventional half-wave dipole antenna used in microwave engineering. We note that the most common dielectrics and semiconductors have a dielectric constant hardly in excess of 10 giving rise to confinement at resonance smaller than 10. Similarly, although $\lambda_{res}/D > 50$ is theoretically possible for $\varepsilon' > 3000$ no such natural material is available to the best of our knowledge. However, very high indices are accessible in the microwave regime close to polar resonances in ferroelectrics or the Reststrahlen band in polar crystals [35, 36]. As stated earlier, we are interested in those resonances for which $\eta \geq 50\%$,

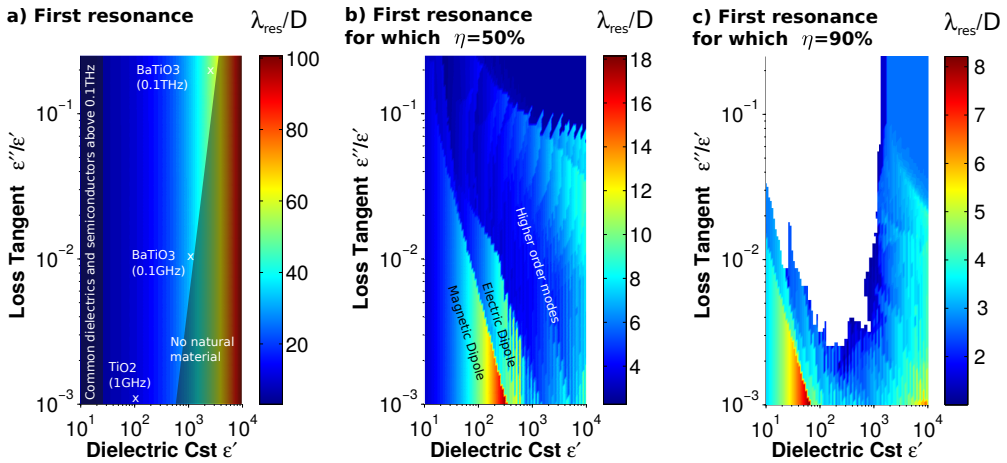

Fig. 1. a) Resonance wavelength λ_{res} of the first order mode for a dielectric sphere of radius $R = D/2 = 10\,\mu$m as a function of its permittivity given by equation 1 with the dielectric constant and loss tangent varying logarithmically along the horizontal and vertical axis respectively, b) resonance wavelength of the lowest energy mode for which $\eta \geq 50\%$ and c) $\eta \geq 90\%$ for the same dielectric sphere.

a condition which modifies considerably the picture as shown in Fig. 1b. Note that this corresponds to a ratio $Q_{scat}/Q_{abs} \sim 1$. One can see that the best miniaturization is achieved at low losses, for the magnetic dipole mode, and is maximum at $\lambda_{res}/D \sim 16$. At this maximum value, the extinction efficiency Q_{ext} can be as high as 80. A more efficient system with $\eta \geq 90\%$ ($Q_{scat}/Q_{abs} \sim 10$) is also shown in Fig. 1c which reduces even further the achievable miniaturization, to about $\lambda_{res}/D \sim 7$ ($Q_{ext} \sim 50$). For lower tolerances on loss, such as $\eta \geq 99\%$, there is close to no acceptable $\tan\delta$ for the parameter space probed and one is limited by the quality of materials. This condition brings also the miniaturization closer to the microwave limit of $\lambda_{res}/D \sim 2$ so that there is little gain compared to using the sophisticated designs which have been developed for perfect electric conductor (PEC) at low frequencies. This conclusion also stands for conductors and polar materials but there the range of acceptable parameters is much more extended or non-existent making them quite robust or unsuitable, respectively.

Next we study the potential of conductors according to equation 2 with $\varepsilon_\infty = 1$ and $\omega_p = 2\pi \cdot 1200\,$THz ($\lambda_p = 0.25\,\mu$m) varying the size of the particle, see Fig. 2a. One can see that the maximum confinement is much more limited than for HID, nonetheless the global result when imposing $\eta \geq 50\%$ and 90%, see Fig. 2b and c, is very comparable at about $\lambda_{res}/D \sim 16$ for $D = 0.12\lambda_p$ with $Q_{ext} \sim 80$ and $\lambda_{res}/D \sim 7$ for $D = 0.26\lambda_p$ with $Q_{ext} \sim 40$ respectively. When ε_∞ is increased to 10, the resonances are markedly redshifted, although this improves the miniaturization factor for the first resonance, the increased size mismatch with the wavelength of light translates into a reduced Q_{sca}, see Fig. 7. This leads to λ_{res}/D, Q_{ext} and λ_p/D being halved compared to the free-electron case ($\varepsilon_\infty = 1$) for $\eta \geq 50\%$ and 90%.

Last, let us look at a polar crystal with $\varepsilon_\infty = 1$, $\omega_{TO} = 2\pi \cdot 10\,$THz and $\omega_{LO} = 2\pi \cdot 12\,$THz ($\lambda_{LO} = 25\,\mu$m), see equation 3. Thanks to the strong dispersion towards the TO phonon, light compression is an order of magnitude stronger than for conductors with a 10 times larger particle, see Fig. 3a. The trade-off for a dominating scattering contribution is comparable to that of a conductor though, at about $D = 0.12\lambda_{LO}$ and $0.27\lambda_{LO}$ for $\eta \geq 50\%$ and 90%. Unfortunately, the narrow spectral region for which $\Re\{\varepsilon\} < 0$ together with the absorption line of the TO mode reduce dramatically λ_{res}/D to 8 and 3.5 and Q_{ext} to 25 and 8 respectively. Because of

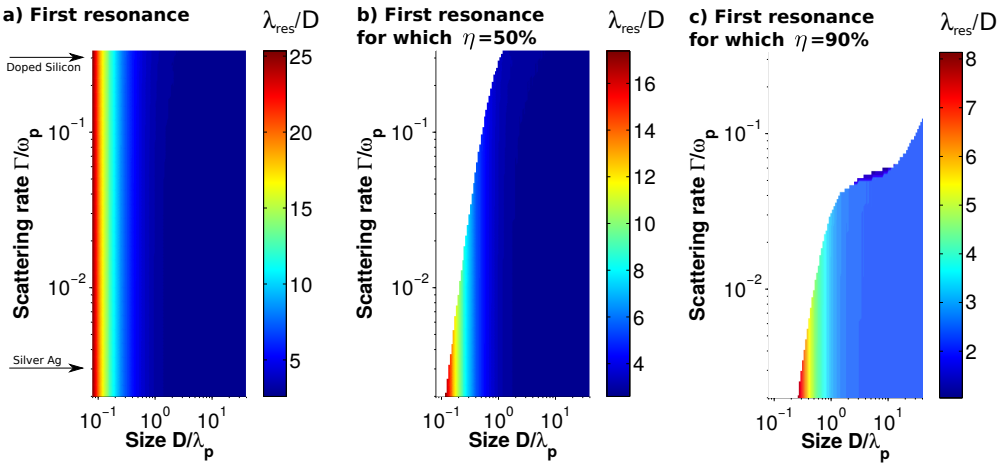

Fig. 2. a) Resonance wavelength λ_{res} of the first order mode for a conducting sphere with a permittivity given by equation 2 with $\varepsilon_\infty = 1$ and $\omega_p = 2\pi \cdot 1200\,\mathrm{THz}$ ($\lambda_p = 0.25\,\mu\mathrm{m}$) in function of its diameter D and scattering rate Γ, b) resonance wavelength of the lowest energy mode for which $\eta \geq 50\%$ and c) $\eta \geq 90\%$ for the same conducting sphere.

the restricted permittivity range available in a polar crystals, the effect of ε_∞ or the backgroud index is rather limited.

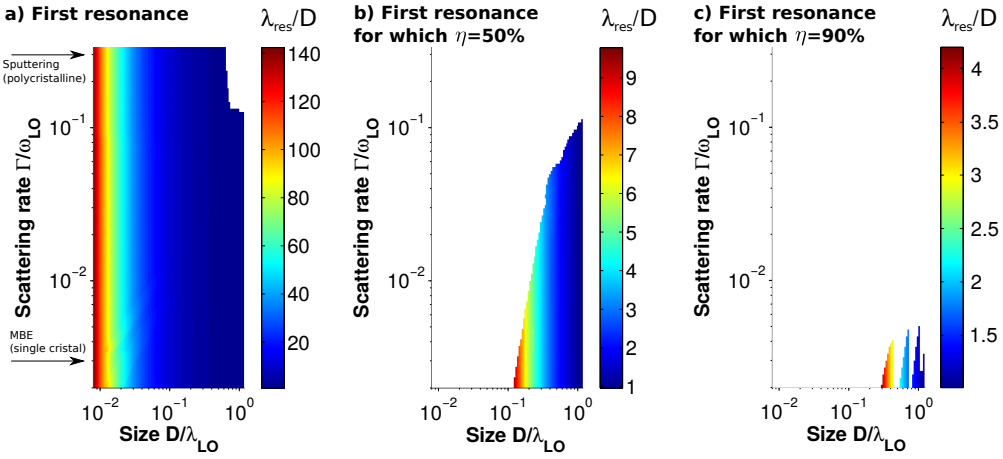

Fig. 3. Resonance wavelength λ_{res} of the first order mode for a polar sphere with a permittivity given by equation 3 with $\varepsilon_\infty = 1$, $\omega_{LO} = 2\pi \cdot 12\,\mathrm{THz}$ ($\lambda_p = 25\,\mu\mathrm{m}$) and $\omega_{TO} = 2\pi \cdot 10\,\mathrm{THz}$ in function of its diameter D and scattering rate Γ, b) resonance wavelength of the lowest energy mode for which $\eta \geq 50\%$ and c) $\eta \geq 90\%$ for the same polar sphere.

3.2. High aspect ratio particles

We now turn to elongated rods as this is, after an increase in size, the most typical way of redshifting further the optical response of scatterers [7]. In the following calculations, the polarization is always directed along the largest dimension of the particles, which we refer to as length.

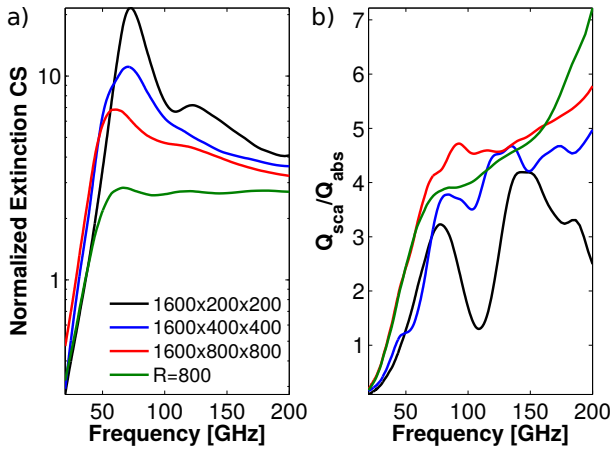

Fig. 4. a) Extinction efficiencies Q_{ext} of a $D = 1600\,\mu$m $BaTiO_3$ spherical particle (green) compared with $BaTiO_3$ antennae with length $L = D$ and square cross-section of 800×800 (red), 400×400 (blue) and $200 \times 200\,\mu\text{m}^2$ (black). b) Relative radiation efficiency Q_{scat}/Q_{abs} for the same antennae than in a).

Fig. 4a plots the extinction efficiency of a sphere with $D = 1600\,\mu$m in the high gigahertz range made out of barium titanate ($BaTiO_3$, $\varepsilon = 2000 + 500i$ [36]) as calculated by FDTD. One can clearly see that as the aspect ratio of the particle is increased from the sphere (black curve) to thin bars with cross-sections 800×800 (blue), 400×400 (red) and $200 \times 200\,\mu\text{m}^2$ (green), the lowest energy resonance narrows down and strengthens, however, its spectral position blueshifts, rather than redshifts, if anything. This is because the resonance wavelength of a dielectric cavity is mostly defined by the index of the material and its size. More, we note that the relative radiation efficiency Q_{sca}/Q_{abs} does not improve with a change of the particle shape for that lowest energy mode, see Fig. 4b.

The picture can become somewhat complicated if one studies materials with a negative permittivity such as conductors and polar dielectrics, because they support localized modes which are highly dependent on the shape of the particle [7]. Nonetheless, if we consider rods with a circular cross-section, it is possible to make use of Novotny's approach [22] which was recently extended to absorbing materials by Demetriadou and Hess [37] where we use the z_4 solution which is the only one to bear physical sense. This effective wavelength theory consists in a scaling of the microwave half-wave antenna formula $\lambda_0 = 2L$ by determining the velocity factor k_0/γ which satisfies $\lambda_{eff} = 2L$ where $\lambda_{eff} = \lambda_0 k_0/\gamma - 4R$ with $k_0 = 2\pi/\lambda_0$ the wavevector of light in free space and R the radius of the rod. In that framework, one is looking for the highest possible λ_0/λ_{eff} ratio which translates into a strong miniaturization factor. Fig. 5a reports the expected confinement for conducting rods with the same permittivity considered before for different radii $R = 5 - 200$ nm. Because of the skin depth effect, thinner wires allow a stronger compression of the light as is well-known from plasmonics [22]. More specifically, a conducting rod with $R = 5$ nm leads to a miniaturization $\lambda_0/L = 8$ (*i.e.* $\lambda_0/\lambda_{eff} = 4$). One can therefore conclude that rods can not achieve as high a scaling as that offered by the small spheres presented in Fig. 2. Note that the asymptotes at small wavelengths arises from the breakdown of the assumption of wires $R << L$.

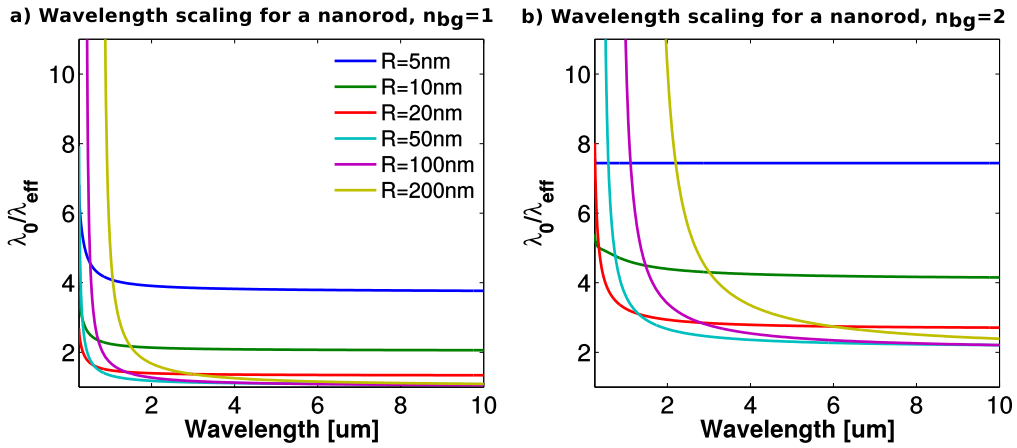

Fig. 5. a) Effective wavelength scaling λ_0/λ_{eff} for a conducting nanorod with a permittivity given by equation 2 with $\varepsilon_\infty = 1$, $\omega_p = 2\pi \cdot 1200\,\mathrm{THz}$ ($\lambda_p = 0.25\,\mu\mathrm{m}$) and $\Gamma = \omega_p/500$ in function of its radius R in a background with index a) $n_{bg} = 1$ and b) $n_{bg} = 2$. Note the asymptotes towards short wavelengths which originate from the breakdown of the assumption of a nanorod, *i.e.* $D << L$.

3.3. Effect of a background index

To terminate this overview on the miniaturization capabilities of radiating antennae, we investigate the effect of the background index and the redshift accompanying the coupling between multiple elements for the case of conductors. Dielectric resonances are dependent on the index contrast, as such an increase in the background index or the presence of a substrate will only lead to a reduced wavelength compression [38]. Furthermore, as we showed earlier, the resonance wavelength in these systems is given by the total length, therefore the resonance of assemblies can only be at equal or higher energy than that of the spheres discussed before. On the other hand, polar materials are hampered by the strong TO absorption line and hence redshifting mechanisms are either detrimental or of little effect.

Back to conductors, we see that an increase in the background index redshifts most strongly the resonance of the smallest particles as expected, see Fig. 8a, resulting in up to a factor $\sim n_{bg}$ increase for those. As the particle size increases, the effect weakens and almost disappear for the largest spheres. The presence of a substrate rather than a homogeneous background would have an even more limited effect. When one imposes the condition $\eta \geq 50\%$ and 90%, the miniaturization is not improved by the background index nor is it much undermined, see Fig. 8b and c. The optimum size is simply shifted to $D = 0.25\lambda_p$ and $0.6\lambda_p$ while $Q_{ext} \sim 60$ and 25, respectively. This stems from the exponentially decaying dependence on the background index as the size of the particle increases.

In the case of the conducting rods, see Fig. 5b, the shift is largest for the thinnest particles, again as expected, with a shift also comparable to $\sim n_{bg}$ for $R = 5\,\mathrm{nm}$. As a side note, let us highlight the interesting fact that a conductor with increased loss (larger Γ) exhibits a stronger plasmonic behaviour leading to an improved wavelength compression, see Fig. 9. However, one should pay attention to the radiation efficiency η in that case, as it is not considered in our simple effective wavelength analysis. This can be fully taken into account by the model developed by Dorfmüller *et al.* [39, 40] to which we direct the interested reader but is beyond the scope of the present article.

3.4. *On the assembly of particles*

It has been shown recently by Li and co-workers [41] that an alternative route to the miniaturization of antenna can be achieved by placing small elements in conductive contact to each others, see Fig. 10 for an example. This can give rise to an additional 200% wavelength scaling under optimal circumstances and up to 300% if one uses core-shell instead of plain particles. The individual particles are also more sensitive to the background index than the equivalent rod enabling strong redshifting mechanisms, as shown in Fig. 10. However, this method poses two important problems. The first and most obvious issue is that the fabrication and assembly of touching spheres is long and tedious. The second aspect is more treacherous and is related to the radiation efficiency η. To illustrate this issue, we calculated by FDTD the cross-sections of five touching spheres and a rod of equal diameter and equivalent total length ($L = 5 \times D$) made out of a conductor with a permittivity close to that of indium antimonide ($m^* = 0.014 \cdot m_e$, $\varepsilon_\infty = 16$, $N = 10^{16}\,\mathrm{cm}^{-3}$ and $\Gamma = \omega_p/10$) [42], see Fig. 6a. Note that the polarization is aligned along the bars and particle chains. As one can see, although the extinction efficiency is smaller for the

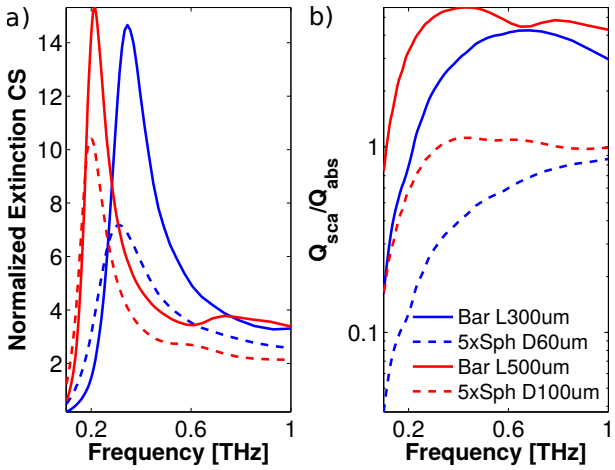

Fig. 6. a) Extinction efficiencies Q_{ext} of 5 touching InSb spherical particles with $D = 60$ (blue dashed) and $D = 100\,\mu$m (red dashed) compared with InSb antennae with respective length $L = 5 \times D$ and square cross-section of $D \times D$ (full lines). b) Relative radiation efficiency Q_{scat}/Q_{abs} for the same structures than in a).

sphere assembly, its first resonance is located at lower energy that that of the equivalent rod. But more importantly, because of the greater size mismatch between the individual spheres and free-space light than between the latter and the rod, the relative scattering contribution is much smaller than the absorption for the assembly, see Fig. 6b. Furthermore, by considering a size of the individual nanoparticles which leads to $Q_{sca}/Q_{abs} \sim 1$ ($D = 100\,\mu$m) or $Q_{sca}/Q_{abs} < 1$ ($D = 60\,\mu$m), we conclude that the assembling cannot improve nor modify notably the radiation efficiency. Indeed, we see that in both cases Q_{sca}/Q_{abs} is largely unaffected by the assembling compared with the single sphere. At the opposite, the rods are much more efficient with a strong scattering contribution. This means that as long as radiating antennae are concerned, the method of assembly is not favourable.

4. Conclusion

In this contribution, we identify the dimensionless physical quantities which allow us to describe and compare optical antennae made out of three categories of materials: polar crystals,

high index dielectrics and conductors. Although the physical principles at the origin of their strong optical properties differ, comparable behaviour are observed for all three cases. This is particularly true when one considers antennae for which the radiative contribution dominates. Furthermore, we show that in this situation the ratio between the wavelength of light and the antenna size is below 20 in all cases (it is 2 in the microwave regime) including all possible redshifting mechanisms such as that of shape, background index or coupling (assembly). Strikingly, and contrary to expectations, we see that conductors are still the best optical materials for the fabrication of radiative miniaturized antennae when all factors are taken into account. These conclusions bring an interesting perspective on the current trends in state-of-the-art nanophotonics and provides us with the upper achievable limits in antenna miniaturization.

Appendix A

In this appendix, we present additional figures showing the variation of the miniaturization factor caused by an increase of the high frequency permittivity ε_∞ (Fig. 7) or the background index (Fig. 8) for conducting spheres or the losses (Fig. 9) for conducting wires. We also reproduce in Fig. 10 and expand on the results of Li and co-workers [41] highlighting the additional shifts induced by replacing a gold bar (full lines) by an assembly of five touching spheres (dashed lines) with equivalent total length and light polarised along it. These two systems are placed in air (black curves), on glass (blue curves) and in glass (red curves). Note furthermore, that this figure considers periodic arrays from which only the transmittance is extracted thus overlooking changes in the ratio between radiative and absorbing contributions which are discussed in detail in Fig. 6 for a similar system.

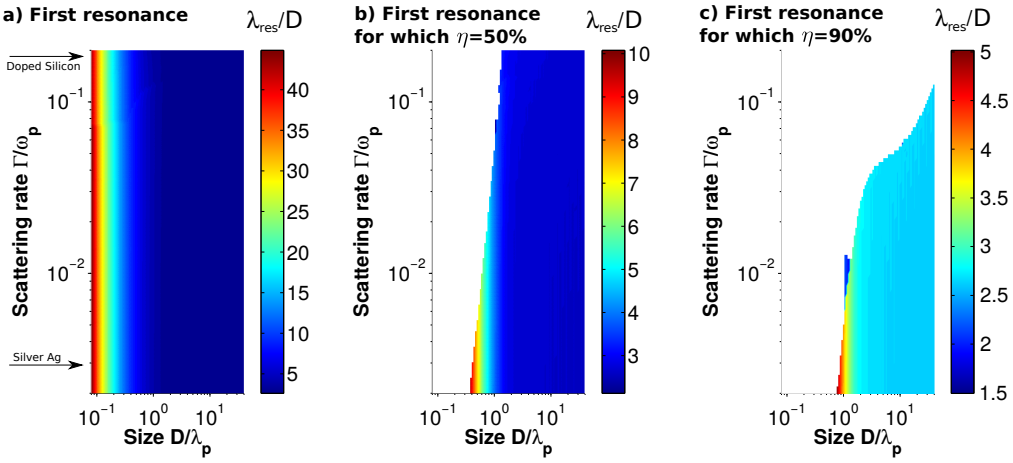

Fig. 7. a) Resonance wavelength λ_{res} of the first order mode for a conducting sphere with a permittivity given by equation 2 with $\varepsilon_\infty = 10$ and $\omega_p = 2\pi \cdot 1200\,\mathrm{THz}$ ($\lambda_p = 0.25\,\mu\mathrm{m}$) in function of its diameter D and scattering rate Γ, b) resonance wavelength of the lowest energy mode for which $\eta \geq 50\%$ and c) $\eta \geq 90\%$ for the same conducting sphere.

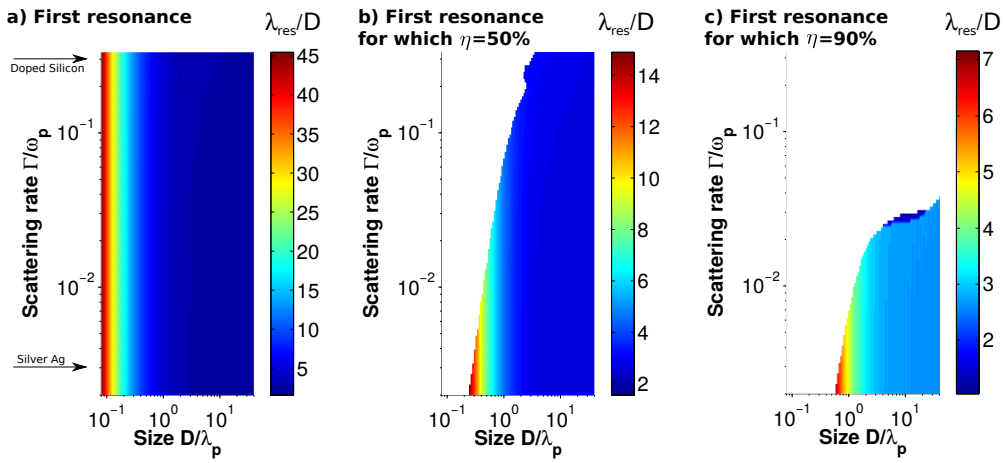

Fig. 8. a) Resonance wavelength λ_{res} of the first order mode for a conducting sphere with a permittivity given by equation 2 with $\varepsilon_\infty = 1$ and $\omega_p = 2\pi \cdot 1200\,\mathrm{THz}$ ($\lambda_p = 0.25\,\mu\mathrm{m}$) in a background index $n_{bg} = 2$ in function of its diameter D and scattering rate Γ, b) resonance wavelength of the lowest energy mode for which $\eta \geq 50\%$ and c) $\eta \geq 90\%$ for the same conducting sphere.

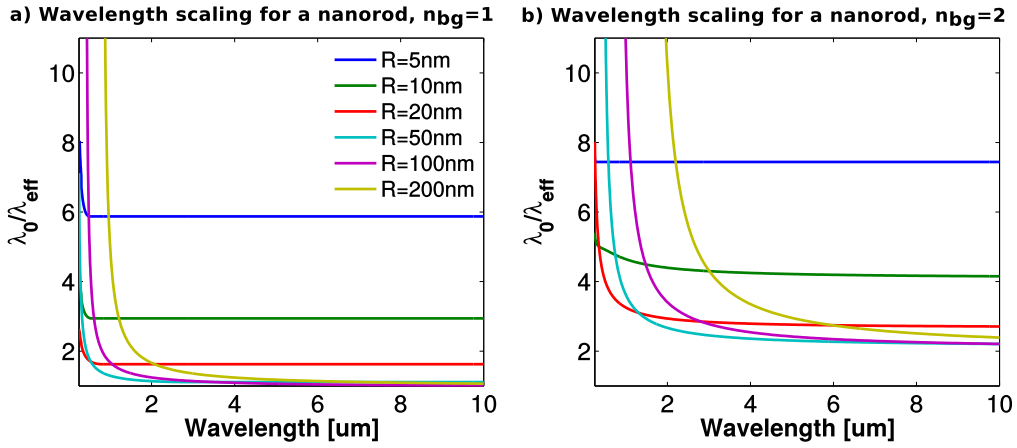

Fig. 9. a) Effective wavelength scaling λ_0/λ_{eff} for a conducting nanorod with a permittivity given by equation 2 with $\varepsilon_\infty = 1$, $\omega_p = 2\pi \cdot 1200\,\mathrm{THz}$ ($\lambda_p = 0.25\,\mu\mathrm{m}$) and $\Gamma = \omega_p/3$ in function of its radius R in a background with index a) $n_{bg} = 1$ and b) $n_{bg} = 2$. Note the asymptotes towards short wavelengths which originate from the breakdown of the assumption of a nanorod, *i.e.* $D << L$.

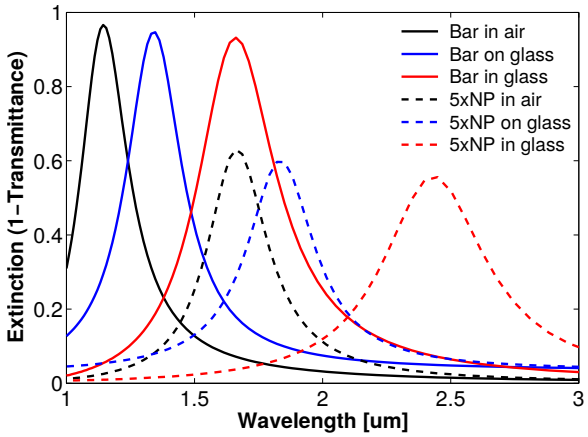

Fig. 10. Extinction of a periodic array ($\Lambda_x = \Lambda_y = 600\,\text{nm}$) of 5 touching Au spheres (dashed lines) with $D = 60\,\text{nm}$ in air (black), on glass (blue) and in glass (red) compared with their respective equivalent Au rods (full lines) with $L = 5 \times D$ and square cross-section $D \times D$.

Acknowledgments

Y.F. and S.M. acknowledges support from the UK Engineering and Physical Sciences Research Council (EPSRC). J.Y. and M.H. would like to thank the National Natural Science Foundation of China (Grant Nos. 61161007, 61261002) and China Postdoctoral Science Foundation (Grant No. 2014T70890).